

Figure 9.35 Mixture size analysis

Three tests were conducted on the BBA material supplied, two at about $C_w = 19\%$ and the third at $C_w = 35,3\%$. The friction gradients obtained are illustrated in Figs 9.36 and 9.37. It is interesting to note that there is a fairly large difference between the friction gradients recorded for the two similar concentration tests.

A possible explanation for this discrepancy is the change in size distribution between the two tests. (Table 9.38).

Table 9.39 Size analysis of the BBA samples taken during each pumping test

Sieve size (µm)	Cumulative percentage passing (%)			
	Original material	Test A $C_w = 19,4\%$	Test B $C_w = 19,3\%$	Test C $C_w = 35,3\%$
6300	94,1	98,1	99,3	96,9
4750	91,7	96,3	98,7	95,3
2360	83,0	88,0	93,4	88,1
1180	69,7	73,2	82,5	74,8
600	56,4	57,1	67,9	60,1
212	30,6	33,6	43,1	36,9
106	10,5	14,4	20,7	16,4

The above size distributions are illustrated in Fig. 9.38. Test A was conducted on completion of the mixing of the BBA and water in the pumping system. The mixing/filling procedure takes in the region of 1 hour and the test a further hour. The material was circulated through the pumping circuit for a number of hours prior to test B. The result of this, is a shift of the d_{50} from 483 μm to 320 μm . This shift in the size distribution is considered to be the main contributing factor to the discrepancy between the two results. This particle size shift and corresponding pressure gradient shift is dealt with in the analysis of the results.

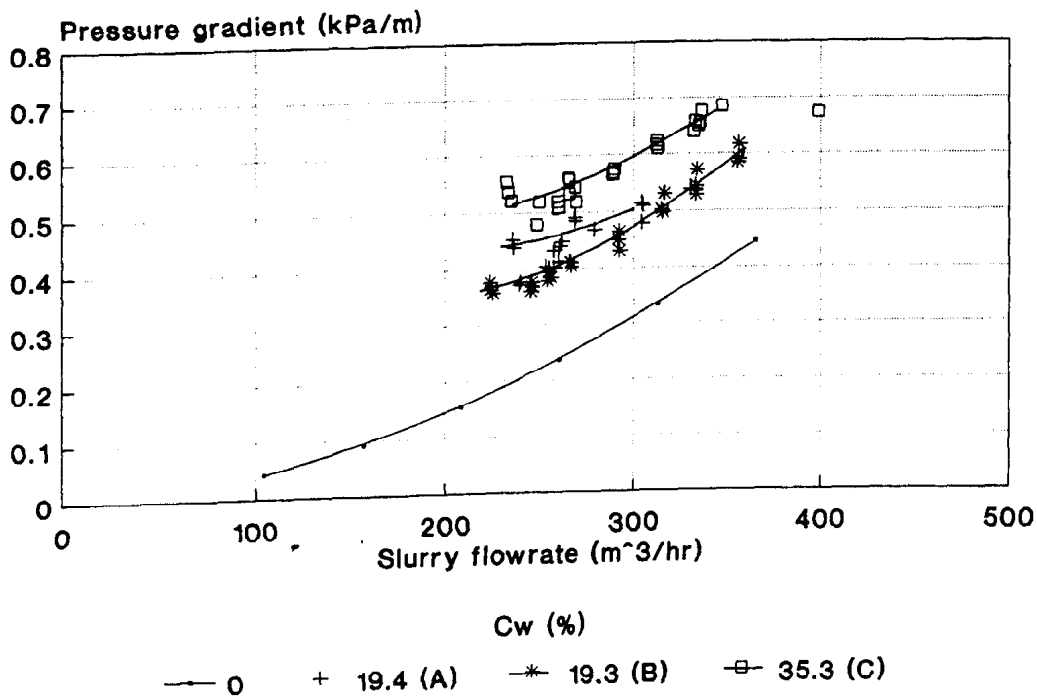


Figure 9.36 BBA predictions (rubber)

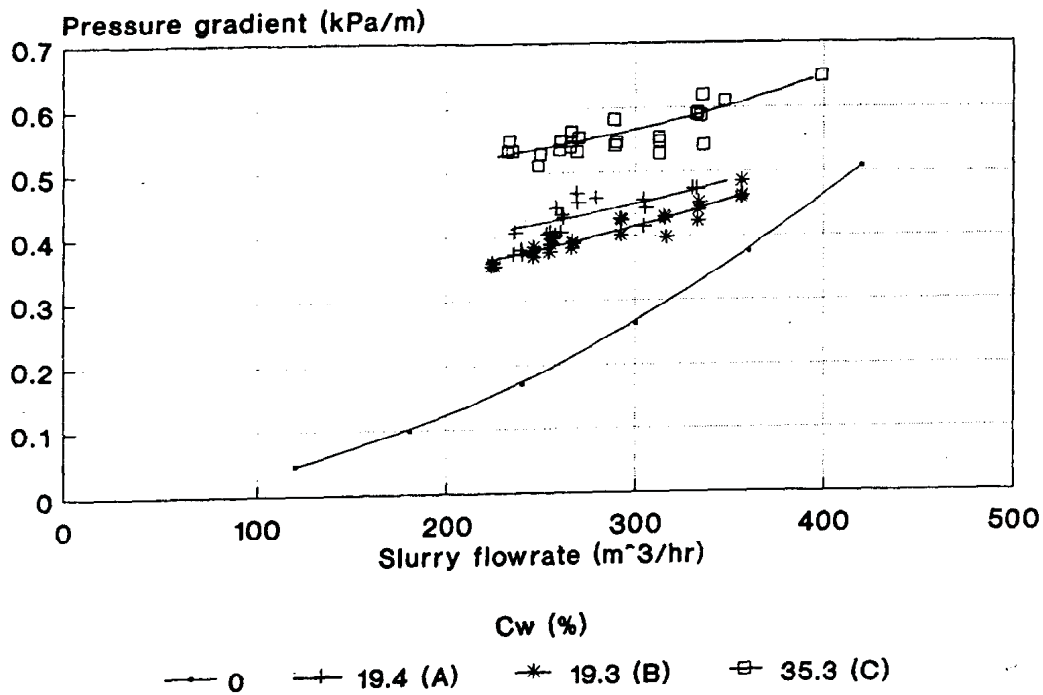


Figure 9.37 BBA predictions (steel)

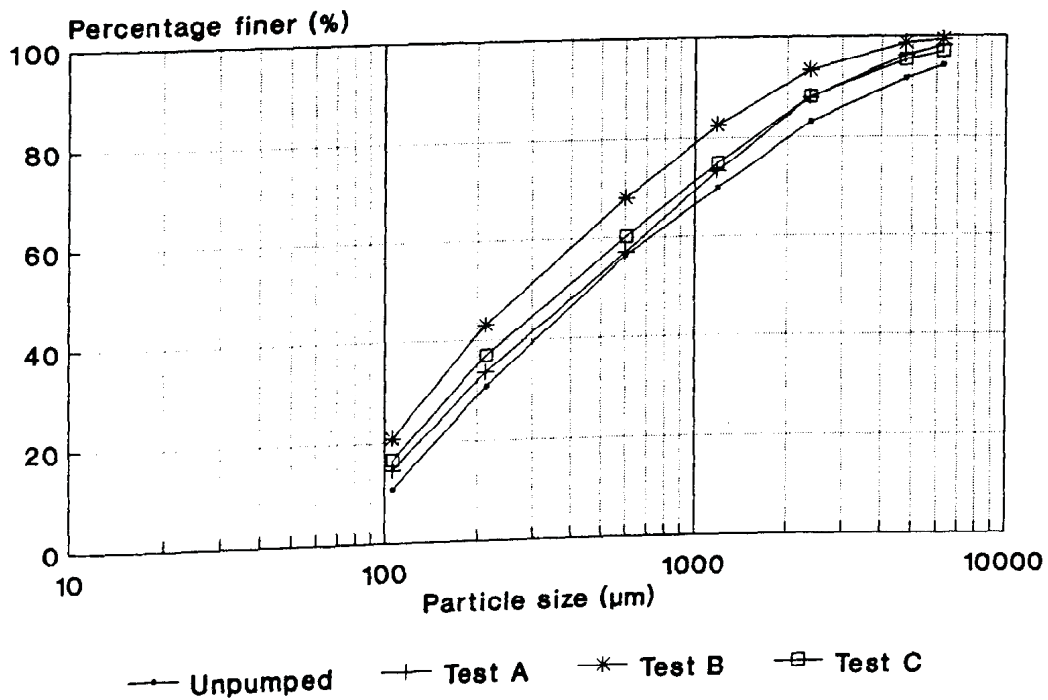


Figure 9.38 BBA size distributions

The material for Test C was obtained by combining the BBA after test B with a fresh batch of BBA to increase the slurry concentration up to 35%. The size analysis for Test C indicates a similar distribution to Test A. Both analyses are within 5% of the total cumulative percentage passing for each sieve size of the original sample.

The friction gradient curves of the BBA slurries indicate a flattening out near deposition and an asymptotic tendency towards the water curves at the higher velocities. This is typical of a heterogeneous type slurry.

The onset of deposition for the various slurries was obtained by visually monitoring the progress of the slurry through a transparent viewing section in the pipeline.

The prevalent conditions within the pipeline for each pump speed were monitored and used to estimate the onset of saltation and deposition. The conditions and the corresponding pipeline velocities are included in Table 9.40.

As can be derived from Table 9.40 below, the inclusion of BBA increases the critical deposition velocity. The settling tests in the 212 mm section indicates that deposition occurs in the range of 0,67 - 1,04 m/s for the range of concentrations tested for the PFA slurries.

Table 9.40 Prevalent conditions in the 212 mm View section for the different velocities recorded

Test material	C _w (%)	Pipeline flowrate (m ³ /hr) (Velocity (m/s))			Deposited bed
		First Indications of irregular flow	Saltation		
			Upper	Lower	
PFA	43,6	224,5 (1,78)	172,8 (1,36)	115,1 (0,91)	
PFA	47,7	229,5 (1,82)	182,7 (1,44)	106,0 (0,84)	
PFA	53,1	212,9 (1,69)	133,2 (1,05)	103,8 (0,82)	84,7 (0,67)
PFA	56,5	206,9 (1,64)	156,3 (1,23)	130,8 (1,04)	102,7 (0,82)
BBA:PFA 1:4	51,5	211,5 (1,67)		150,3 (1,18)	140,3 (1,10)
BBA:PFA 1:2	49,5	235,7 (1,86)		188,0 (1,48)	166,0 (1,31)
BBA:PFA 1:1	50,0			212,2 (1,67)	202,2 (1,59)
BBA:PFA 1:1	40,7	240,9 (1,92)		230,4 (1,81)	215,1 (1,69)
BBA	19,4	262 (2,06)		256,0 (2,01)	240,7 (1,89)
BBA	19,3	268,2 (2,11)		256,4 (2,02)	246,7 (1,94)
BBA	35,3			250,5 (1,97)	236,5 (1,86)

Saltation for the PFA slurries occurs within a range of 0,82 to 1,44 m/s. The saltation range is indicated by streaks of black material rolling along the bottom of the pipeline in a wavy pattern to a stop-go situation of wider black streaks just before deposition.

The first apparent visible indications of irregular flow was observed to occur in the range of 1,64 - 1,82 m/s. This observation is however subjective and is character-

ised by the odd particle displaying an irregular wavy pattern on the internal pipe surface.

The deposition velocity range increased as the percentage of BBA in the mixture was increased. At a concentration of about 50%, the deposition velocity range varied from 1,10 - 1,18 to 1,59 - 1,67 to 1,69 - 1,81 for the 4:1, 2:1 and 1:1 ratios respectively.

The influence of the carrier 'viscosity' and its allied support characteristics appears to reach a limiting concentration in the concentration range of 40% - 50% for the 1:1 slurry. The 40% slurry appeared to have a higher deposition velocity than the 50% slurry. This indicates that the 1:1 ratio slurry is more dependent on the concentration, the turbulence and the allied suspension characteristics.

The highest deposit velocity range was experienced with the BBA slurries. The concentration did not appear to have a marked effect on the deposition velocity over the C_w range tested. The deposition tests with the BBA slurries however revealed a quick transition from full flow conditions to flow with a settled bed. This transitional zone became larger as the percentage of PFA was increased. This would appear to enhance the theory that the smaller particles' rheological characteristics enhance the support characteristics of these slurries.

The stability of these slurries is limited by the inadequate yield stress characteristics of the PFA carrier. If the theoretical maximum diameter of a particle which could be sustained in a Bingham fluid is considered viz:

$$\Gamma_y \geq 0,1 \text{ pw gd } (S_s - S_{mca}) \quad (5.160)$$

then it can be clearly seen that these mixture slurries will settle out if sufficient turbulence is not present. The d values calculated for the mixture slurries are included in the following Table.

Table 9.41 d estimations for the BBA:PFA mixtures tested

Mixture ratio (BBA:PFA)	Carrier C_w (%)	Carrier Γ_y (Pa)	d (mm)	Overall slurry C_w (%)
1 : 1	41,1	,133	0,13	50
1 : 2	43,0	,187	0,18	49,5
1 : 4	44,8	,257	0,25	51,5
0 : 1	50	,611	0,64	50

The above results confirm the inadequacy of the rheological characteristics to provide a stable slurry at these concentrations. Higher overall and PFA concentrations nevertheless lead to stable slurries (Section 8,4).

The prediction of the pressure gradients and the deposit velocity is again based on the correlations derived for mixed flow settling slurries. The prediction of the deposit velocity is based on the equations listed in Table 9.11.

There are four main aspects that appear to contribute the most to the determination of the critical deposit velocity, namely, particle size distribution, concentration, slurry 'viscosity' and the degree of turbulence in the slurry.

The equations listed in Table 9.11, generally only address the particle size and concentration aspect, so that deviations can be expected when using them. The critical deposit velocity estimated using these prediction methods are listed in Table 9.42.

Table 9.42 Predicted Deposition velocities (D = 212 mm)

Slurry BBA : PFA	C _w (%)	d ₅₀ (μm)	Critical Deposition velocity (m/s)					
			Approximate experimen- tal value	Wasp 1	Wasp 2	Du- rand 1	Du- rand 2	Ne- witt
0 : 1	53,1	22	0,7 - 0,8	1,33	,98	1,59	1,42	,18
1 : 4	51,5	130	1,1 - 1,18	1,68	1,25	2,28	1,89	1,86
1 : 2	49,5	143	1,31 - 1,48	1,70	1,27	2,31	2,11	1,91
1 : 1	50	177	1,59 - 1,67	1,78	1,33	2,46	2,38	2,18
1 : 1	40,7	177	1,69 - 1,81	1,69	1,33	2,46	2,40	1,90
1 : 0	35,3	431	1,86 - 1,97	1,93	1,58	2,85	2,75	2,87
1 : 0	19,3	320	1,94 - 2,02	1,61	1,51	2,61	2,57	2,22
1 : 0	19,4	483	1,89 - 2,01	1,73	1,56	2,80	2,74	2,13

The data contained in the above Table indicates that there is no one method that satisfies all the slurries. The most universal prediction would appear to be the use of the Durand II equation multiplied by a suitable constant. The constant is obtained by averaging the ratio of the experimental results divided by the Durand II predictions. The value obtained in this manner was found to be 0,73. The predicted values for the deposition velocity using this method is included in the following Table (9.43).

Table 9.43 Derived critical velocity based on the average experimental results

Slurry BBA : PFA	C_w (%)	Average Experimental Value (m/s)	Critical de- posit veloci- ty (m/s)
			Durand III
0 : 1	53,5	0,7 - 0,8	1,16
1 : 4	51,5	1,1 - 1,18	1,38
1 : 2	49,5	1,31 - 1,48	1,54
1 : 1	50	1,59 - 1,67	1,74
0 : 1	35,3	1,86 - 1,97	2,01
0 : 1	19,3	1,94 - 2,02	1,89
0 : 1	19,4	1,89 - 2,01	2,01

This method is slurry specific and is limited by the lack of the inclusion of the rheologically based 'support characteristic' and turbulence of the slurry. This would especially be the case when the 1:1 slurry is considered where the cross-over from the rheological based support and turbulence appears to occur between 40% and 50%.

The prediction of the pressure gradient is again based on the methods listed in Table 9.5. The following assumptions are however included in the rheologically based derivations.

- 1) The BBA slurries are considered to have Newtonian rheology as there is only a small percentage of material below 100 μm .
- 2) The non-Newtonian model is based on the rheology established from the viscometer tests on this slurry (Section 7.4.1).
- 3) The rheology of the mixture slurries is based on the PFA 2 slurry rheology but adjusted to account for the inclusion of a relatively speaking rheologically

inactive BBA component. This is achieved by considering the relative -212 μm fraction to be represented by the PFA 2 rheology. This 'carrier' concentration is based on the excess of the water remaining after the BBA adsorption and absorption characteristics had been taken into account. The C/C_A prediction is based on the use of the effective pipeline viscosity.

- 4) The K value in the Durand component is adjusted until the flattening out of the pressure gradient curve coincided with the flattening or minimum characteristic of the predicted curve and was found to equal 150 for the PFA and mixture slurries.

The friction gradients estimated are included in the following Tables (9.44 - 9.47) for the slurries listed in Table 9.42 for the calculation of the critical deposit velocities. The appropriate size distributions obtained from each test are utilized in the predictions. The predictions are furthermore based on the experimental k/D value obtained in Fig. 9.27.

Although the Lazarus and Sive method (Section 5.53) and Wilson's method (Section 5.55) are also applicable to the flow of these slurries, they are not included in the comparison as the sliding friction value required for these methods was not measured during the experimental program.

Table 9.44 Prediction of the friction gradient for a PFA slurry with $C_w = 53,4\%$ flowing in a 192 mm rubberlined pipe

Velocity (m/s)	Pressure Gradient (kPa/m)				
	Average Experimental value	Wasp (Newtonian)	Wasp (Pseudo-plastic)	$i_w \times r.d$	Lazarus
0,5		,099	,041		
1,0	0,6	,10	,106	,061	,061
1,5	,17	,170	,202	,129	,129
2,0	,26	,272	,326	,220	,220
2,5	,40	,402	,475	,335	,335
3,0	,55	,557	,65	,471	,471

Table 9.45 Prediction of the friction gradient for a 1:4 (BBA : PFA) mixture with $C_w = 51,5\%$ flowing in a 192 mm rubberlined pipe

Velocity (m/s)	Pressure Gradient (kPa/m)				
	Average Experimental value	Wasp (Newtonian)	Wasp (Pseudo-plastic)	$i_w \times r.d$	Lazarus
0,5		,317	,114	,06	,078
1,0		,292	,186	,13	,191
1,5	0,16	,346	,294	,22	,294
2,0	0,27	,443	,430	,33	,430
2,5	0,38	,573	,589	,47	,589
3,0	0,54	,73	,772	,62	,772
3,5	0,71				

Table 9.46 Prediction of the friction gradient for a 1:2 (BBA:PFA) mixture with $C_w = 49,5\%$ flowing in a 192 mm rubberlined pipe

Velocity (m/s)	Pressure Gradient (kPa/m)				
	Average Experimental value	Wasp (Newtonian)	Wasp (Pseudo-plastic)	$i_w \times r.d$	Lazarus
0,5					
1,0		,407	,125	,06	0,085
1,5	0,18	,344	,186	,13	,144
2,0	0,27	,376	,287	,21	,21
2,5	0,38	,458	,419	,33	,33
3,0	0,51	,575	,573	,46	,46
3,5	0,68	,721	,752	,62	,62

Table 9.47 Prediction of the friction gradient for a 1:1 (BBA:PFA) mixture with $C_w = 50\%$ flowing in a 192 mm rubberlined pipe

Velocity (m/s)	Pressure Gradient (kPa/m)			
	Average Experimental value	Wasp (Newtonian)	$i_w \times r.d$	Lazarus
1,5		,563	,11	,481
2,0	,54	,510	,19	,435
2,5	,53	,537	,30	,461
3,0	,61	,610	,42	,578
3,5	,75	,718	,56	,702

A comparison of the test results and the predicted friction gradients would indicate that the yield pseudo-plastic modified Wasp method is the most representative for the PFA only and the mixture slurries.

The Newtonian Wasp method was found to correlate the BBA experimental data best. The large size of the BBA, made it impossible to conduct viscosity tests in the rotary viscometer. The Wasp method also correlated the $C_w = 19,3\%$ results that had shown to have different size distributions as a result of degradation occurring during the extended pumping period. The comparison of the predictions for the two $C_w = 19,3\%$ BBA slurries are included in Table 9.48.

Table 9.48 Comparison of predicted results using the Wasp method with experimental results in the rubberlined pipe

C_w (%)	Pressure Gradient (kPa/m)			
	Test A 19,4%		Test B 19,3%	
Velocity (m/s)	Average experimental	Wasp	Average experimental	Wasp
2,0	0,43	,432	0,37	,362
2,5	0,47	,465	0,41	,413
3,0	0,55	,538	0,50	,497
3,5	0,64	,639	0,61	,607
4,0		,765		,740

The experimental results obtained from this test series clearly indicates the beneficial aspects of transporting a coarse material in a carrier made up of the liquid and fine materials. At the concentrations tested the slurries are all settling slurries, although it has been shown in Section 8.4 that with a further increase in the overall concentration a stabilized slurry can be achieved.

The standard equation (5.160) (Table 9.41) determining the maximum particle size that can be transported in a stable

flow condition, would appear to require some modification. The concentration range tested and the relative stability of the slurry with regard to limiting the critical deposit velocities, would tend to indicate that the overall determination of the critical deposit velocity is dependent on a number of factors. These include, the concentrations of the carrier component and its allied support characteristics and the size and concentration of the carried particles.

9.7 HMC

These slurry tests were conducted in the same pipes as the tails in Section 9.3. The experimental water curves thus illustrated in Fig. 9.10 are applicable to these tests.

The size analysis of the HMC product is given in Table 9.49 and illustrated in Fig. 9.39.

Table 9.49 HMC size distributions

Size (mm)	Cumulative percentage passing (%)	
	1	2
2,36	100,0	100,0
1,70	99,9	99,7
1,18	99,7	96,9
0,60	97,5	96,0
0,425	96,7	93,9
0,300	94,9	76,9
0,180	75,9	63,1
0,150	65,1	10,1
0,106	9,4	0,6
0,075	0,6	
d_{50} (mm)	0,140	0,139
ϕ_{max} 1 (%)	66,5	66,6
ϕ_{max} 2 (%)	66,2	66,4

The particle specific gravity of the test material was found to be 4,4. The maximum experimental loosely packed packing density was found to occur at $\phi_m = ,55$.

The friction gradients for the tests (Appendix 2C) conducted at $C_w = 25,9\%$, $43,5\%$, $54,1\%$ and $61,4\%$ are illustrated in terms of kPa/m in Fig. 9.40 and in terms of $m_{s1}/100$, in Fig. 9.41.

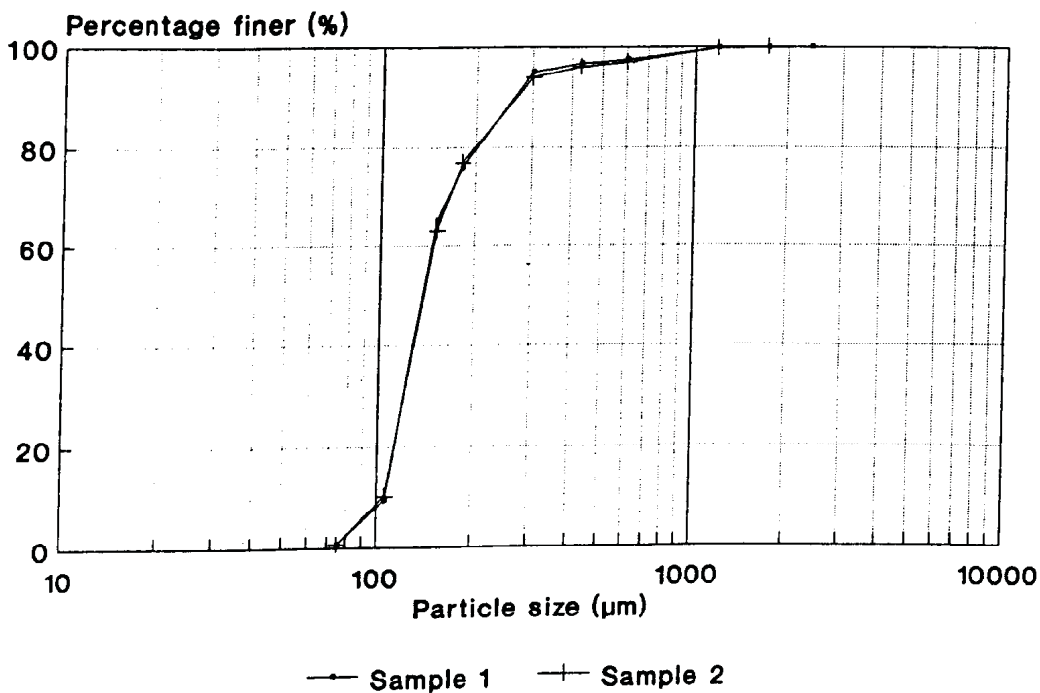


Figure 9.39 HMC Size distribution

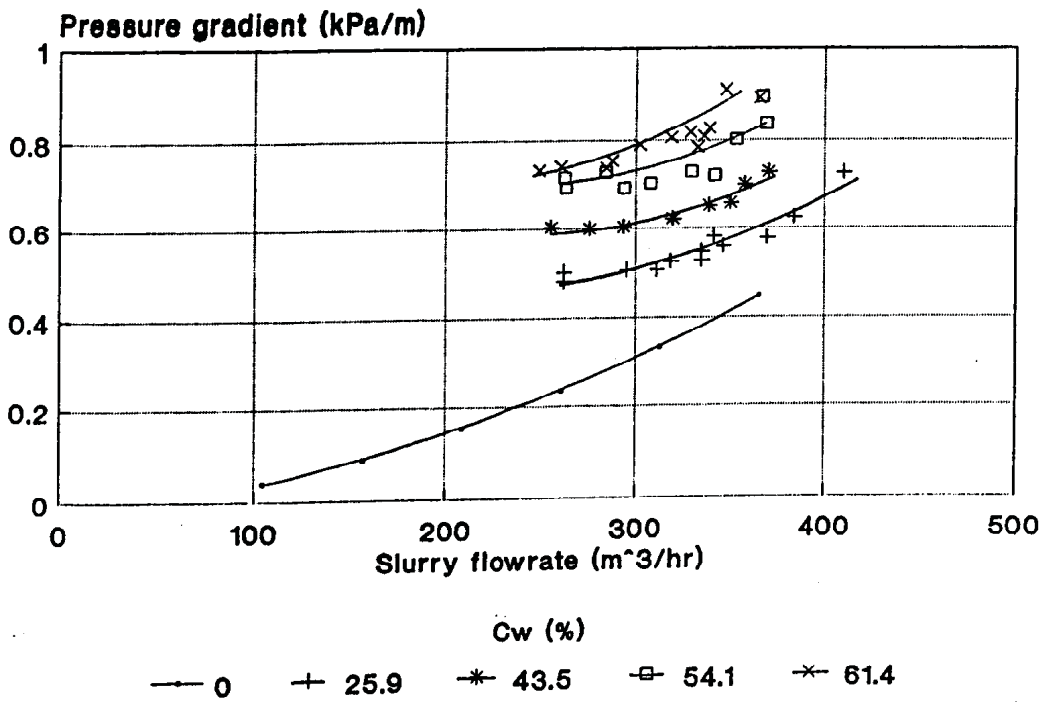


Figure 9.40 HMC Friction gradients (rubber)

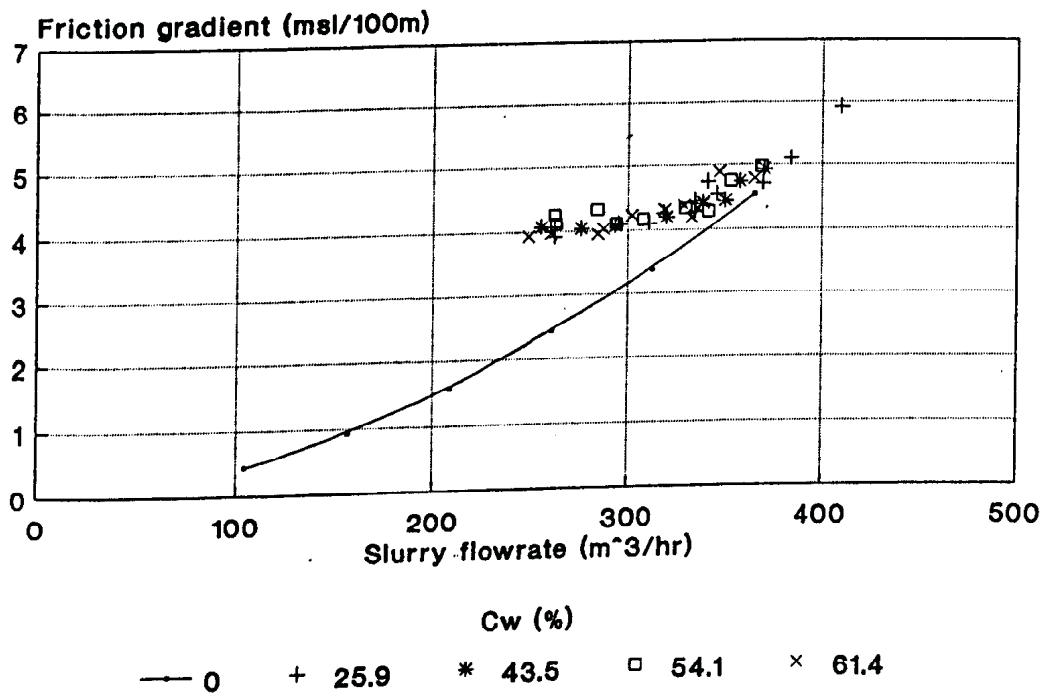


Figure 9.41 HMC Friction gradients (rubber)

The friction gradient results are typical of a heterogeneous type slurry with a flattening out of the curves for each concentration near the deposition velocity and asymptoting towards the water curves at the higher flowrates.

The experimental deposition velocity range is given in Table 9.50.

Table 9.50 Experimental deposition velocity range for the HMC slurries

C _w (%)	Deposition range	
	Flowrate (m ³ /hr)	Velocity (m/s)
25,9	310 - 318	2,44 - 2,50
43,5	293 - 319	2,31 - 2,51
54,1	293 - 329	2,31 - 2,59
61,4	287 - 332	2,26 - 2,61

From the above results it can be seen that there is a general increase in the deposition velocity with an increase in concentration.

This slurry was characterised by similar flow characteristics to the tails 15 slurries within the pipeline, namely a fairly small flow transition to the critical deposit velocity, a changing and biased concentration profile within the pipeline, and an asymptoting friction gradient curve.

It can therefore be expected that the prediction formulae suitable to the tails 15 slurries would be suitable for this slurry. The high specific gravity of the material

resulted in a fast settling slurry so that it was impossible to get a uniformly mixed slurry in the viscometer mix bowl. This made it impossible to conduct representative rheological testwork on the slurries. The apparent heterogeneity of the slurry also indicated that a Newtonian approach could be made in estimating the relative viscosity of the slurries. The predicted friction gradients using the prediction formulæ, based on Lazarus, Durand's and Wasp's formulæ, for the three higher concentration slurries are given in the following Tables (9.51 - 9.53).

Table 9.51 Pressure gradient predictions for a $C_v = 13,5\%$ slurry flowing in a 192 mm rubberlined pipe

Velocity (m/s)	Pressure Gradient (kPa/m)			
	Average Experimen- tal	Wasp*	Lazarus	Durand
2,0			,332	
2,5	0,60	0,60	,442	,564
3,0	0,63	0,64	,558	,599
3,5	0,71	0,73	,682	,670
4,0	0,81	0,85	,855	,769

* $K = 60$ and the viscosity is based on the Roscoe equation

Table 9.52 Pressure Gradient predictions for a $C_v = 54,1\%$ slurry flowing in a 192 mm rubberlined pipe

Velocity (m/s)	Pressure Gradient (kPa/m)			
	Average Experimental	Wasp	Lazarus	Durand
2,0		0,68		
2,5	0,68	0,65	,487	,702
3,0	0,71	0,70	,614	,711
3,5	0,81	0,80	,765	,765
4,0			,970	

Table 9.53 Pressure Gradient predictions for a $C_v = 61,4\%$ slurry flowing in a 192 mm rubberlined pipe

Velocity (m/s)	Pressure Gradient (kPa/m)			
	Average Experimental	Wasp	Lazarus	Durand
2,0			,398	
2,5	0,74	0,64	,531	,821
3,0	0,80	0,71	,670	,808
3,5	0,93	0,84	,828	,847
4,0		1,02		

The maximum volume concentration transported was approximately 48% of the maximum freely packed volume concentration. The slurry concentration could thus possibly have been increased if a more powerful motor had been available.

The predicted values of the critical deposition velocity are contained in Table 9.54.

Table 9.54 The predicted values of critical deposition velocity

C_w (%)	Critical Deposition velocity (m/s)					
	Experimental	Wasp 1	Wasp 2	Durand 1	Durand 2	Newitt
43,5	2,3 - 2,5	2,4	2,1	3,6	3,4	2,6
54,1	2,3 - 2,6	2,6	2,1	3,7	3,5	3,1
61,4	2,3 - 2,6	2,7	2,1	3,8	3,5	3,4

The closest correlation is given by the Wasp 1 prediction. The Durand 1 and 2 correlation can be utilized if multiplied by a suitable factor.

9.8 Comparison of the basic slurry performance characteristics with the average particle characteristics

The experimental results for the medium phase slurry shown in this chapter shows a wide range of performance characteristics. This is clearly shown in the performance curves plotted with the vertical scale plotted as $m_{s1}/100m$.

The settling characteristics of these slurries result in two distinct regions joined by an intermediate region. In the low flowrate regions particle inertia is predominant, resulting in high bed loads with the resulting friction gradient always higher than the base friction curve. The settling characteristics in these low flowrate regions also results in a breakdown of the overall rheological make up of the slurry. This can clearly be seen by the concentration profile occurring within the pipe when the slurry is near settling.

In the high speed areas the viscous effects predominate resulting in friction gradients dependent mainly on the rheology of the slurry. In general it is difficult to interpolate the type of fluid from the turbulent flow of these slurries through pipelines, and as they have settling characteristics it is not possible to transport them in the laminar flow regions.

Two factors can however be utilized in identifying the type of fluid model that could be expected. The size distribution range tested in Chapter 7 gives some indication of the Newtonian/non-Newtonian characterization that could be expected for the slurries tested in this chapter. The size analysis of the slurries tested in this chapter are illustrated in Fig. 9.42 and compared with the finest and coarsest quartz based tailings tested in Chapter 7.

As the PFA 2 tested in this chapter corresponds to the PFA 2 tested in Chapter 7, it can be concluded that the representative rheology obtained would manifest itself in the turbulent flow of the slurries tested in this chapter. This is shown to be the case in Section 9.6.

The quartz based tailings tested in this chapter have larger d_{50} 's than the coarsest tailings product tested in Chapter 7. The products tested here however have similar d_{10} 's to the tails 8 product, and as shown by the rheological tests of the slurries pumped in this chapter non-Newtonian characteristics were again detected, and could be utilized in determining the friction gradients of the slurries.

The larger particle slurries, tails 15, HMC and the BBA could not be subjected to rheological tests as a result

of the size limitation imposed by the viscometer's cup and spindle utilized for all this testwork.

The coarse nature of these slurries and the rheological results obtained from finer slurries however indicate that Newtonian viscosities would occur over the concentration range of the slurries tested in this chapter.

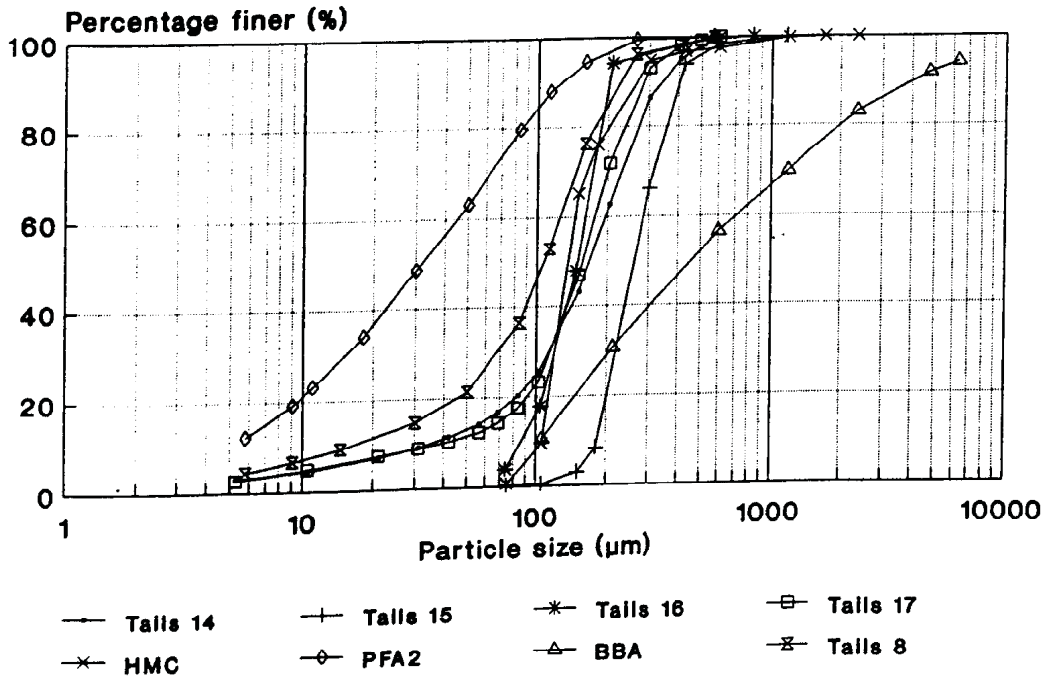


Figure 9.42 Slurry materials size distribution

The particle size range is thus the first indication of the type of flow model that can be expected to influence the performance characteristics of these slurries.

The expected result, can be roughly identified where these slurries have been transported at high velocities. This is due to the fact that each flow model has a characteris-

tic trend in the turbulent flow region.

To illustrate this effect, a pseudo non-settling slurry performance characteristic is determined from an assumed rheogram. The rheogram is based on the relative viscosity at 500 s^{-1} corresponding to the relative viscosity obtained from the Roscoe equation (Table 5.1) and used in most of the Wasp predictions in this chapter.

The composite pseudo rheogram utilized is illustrated in Fig. 9.43 and analyzed in terms of the three non-Newtonian flow models utilized in this thesis. The composite rheogram established in Fig. 9.43 has slightly lower rheological characteristics than the slurries tested in this chapter.

To encompass the range of rheological characteristics in this chapter, flow models are established for the rheograms illustrated in Fig. 9.43 and for a similar rheogram with the shear stresses increased by a factor of 10.

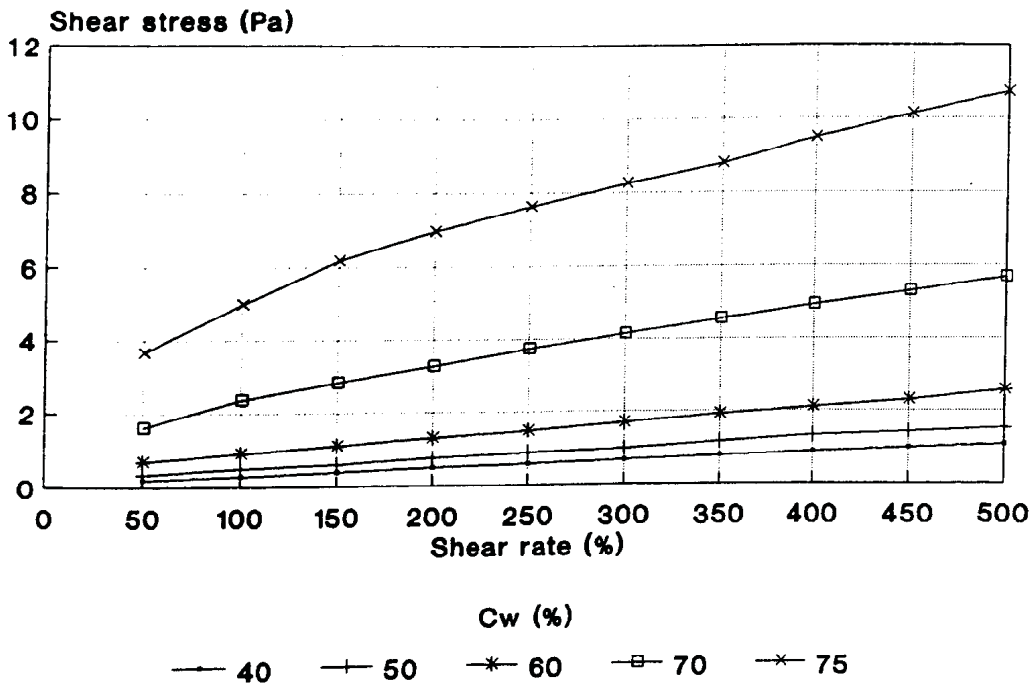


Figure 9.43 Composite rheogram of the assumed rheological characteristics

The flow models fitted to the rheograms represented by the $C_w = 50$ and 60% curves are given in the following Table (9.55). The above concentrations represent the limit of the range of medium phase slurries tested in this chapter.

Table 9.55 Flow models fitted to the assumed rheogram and $10 \times$ assumed rheogram

C_w (%)	Flow model (Pa) Assumed rheology	Correlation coefficient
50	$\Gamma_w = ,223 + 2,685 \text{ E-03 } S$ $\Gamma_w = ,0241 * S^{,6617}$ $\Gamma_w = ,21 + 3,0655 \text{ E-03 } S^{,9805}$ $\Gamma_w = 3,07 \text{ E-3 } S$,9977 ,9878 ,9987
60	$\Gamma_w = ,51 + 3,989 \text{ E-03 } S$ $\Gamma_w = ,07089 S^{,5612}$ $\Gamma_w = ,48 + 5,289 \text{ E-03 } S$ $\Gamma_w = 5,09 \text{ E-3 } S$,998 ,982 ,999

C_w (%)	Flow model (Pa) 10 x Assumed rheology	Correlation coefficient
50	$\Gamma_w = 2,23 + 2,685 \text{ E-02 S}$ $\Gamma_w = ,241 \text{ S}^{,6617}$ $\Gamma_w = 2,10 + 3,0566 \text{ E-02 S}^{,9805}$ $\Gamma_w = 30,7 \text{ E-03 S}$,998 ,988 ,999
60	$\Gamma_w = 5,10 + 3,989 \text{ E-02 S}$ $\Gamma_w = ,7089 \text{ S}^{,5622}$ $\Gamma_w = 4,8 + 5,289 \text{ E-02 S}^{,9556}$ $\Gamma_w = 50,9 \text{ E-03 S}$,998 ,982 ,999

Based on the methodology utilized in Chapter 7, the rheogram illustrated in Fig. 9.43 is best represented by the yield pseudoplastic model. However to illustrate the difference in the friction gradients obtained utilizing the different flow models of similar order of magnitude rheological parameters, all the models are utilized.

The comparative performance curves obtained are based on the friction factors based on the Newtonian Colebrook-White equation⁽¹⁾ and the non-Newtonian Torrance equation (eqn 5.103) which describes the flow of pseudoplastics, Bingham and yield pseudoplastics when utilized with the appropriate rheology and the correct definition of the Reynold's number (Chapter 5).

The friction gradients obtained for $C_w = 50\%$ and 60% slurries assuming the flow of the homogeneous slurry made up of non-settling particles with an s.g. of 2,70 is illustrated in the following flow performance curves (Figs. 9.44 & 9.45). The results used are included in Appendix AD. The curves are for a 100 mm steel pipe and a roughness ratio of 5×10^{-4} . The smooth wall friction factors obtained from the Torrance equation are adjusted for the

roughness ratio by the methods proposed by Govier and Aziz⁽²⁾.

The pseudoplastic model results in a friction gradient curve lower than the water curve for the assumed rheology and substantially lower than the friction gradients obtained from the other 3 models for the assumed and 10x assumed rheology for both the $C_w = 50\%$ and 60% curves.

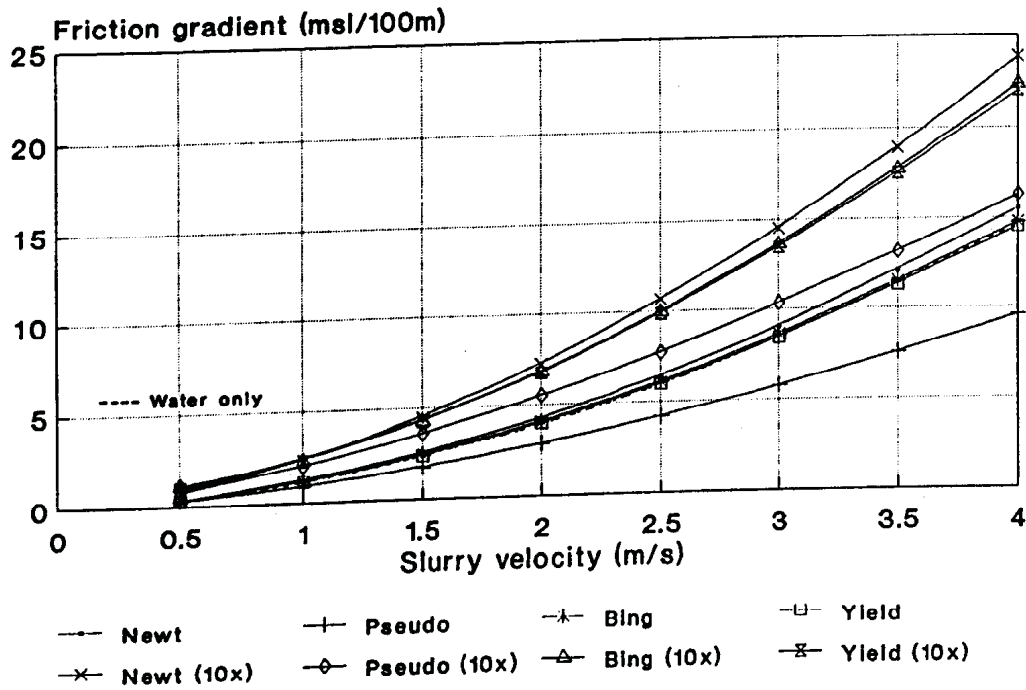


Figure 9.44 Predicted performance characteristics of a pseudo homogeneous slurry with $C_w = 50\%$

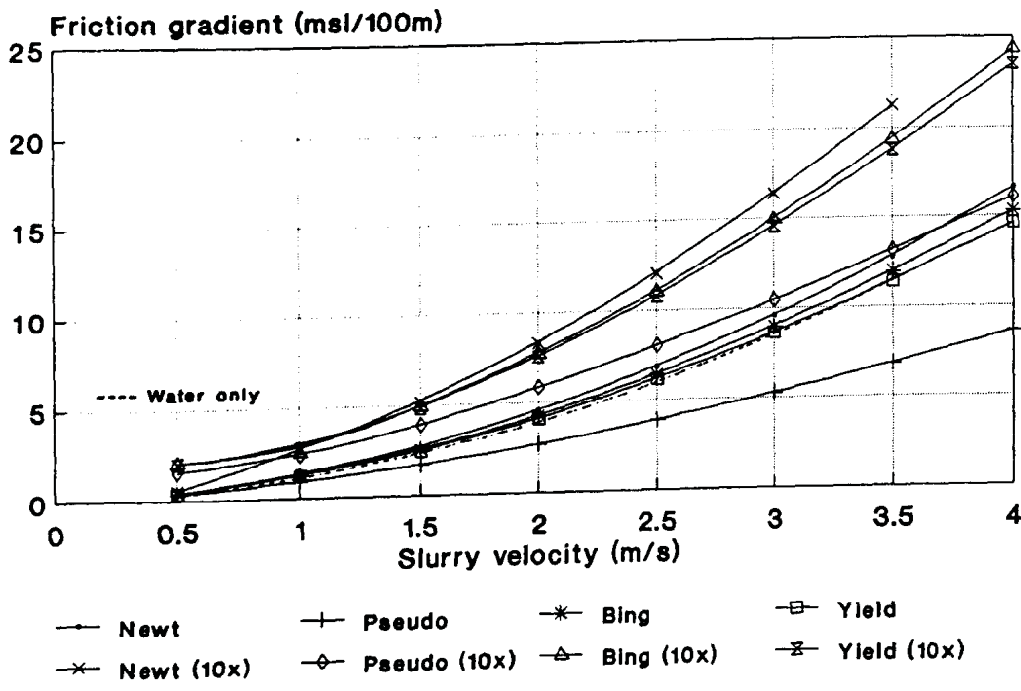


Figure 9.45 Predicted performance characteristic of a pseudo homogeneous slurry with $C_w = 60\%$

The actual results that would be expected for the different slurries pumped are subject however to the actual shape of the rheograms established for each slurry, but the curves shown as a whole give an indication of the trends that could be expected.

The characteristic of the friction gradient curve of a slurry falling under the friction gradient of the water curve occurs with the $C_w = 48\%$ test on tails 14 slurry. The rheogram established for the tails 14 product (Fig. 9.8) indicates that a pseudoplastic response could be expected for the lower concentration slurry. The higher concentration slurries exhibited yield pseudoplastic tendencies and friction gradient curves on or above the water friction gradient curves are thus expected and do in fact occur (Fig. 9.4).

The more typically Newtonian slurries, tails 16, HMC and the BBA displayed strong bed load characteristics over the velocity ranges tested and as such it is difficult to comment on the exact location of the slurry friction gradient curves in the high flowrate regions but the indications are that the curves are on or above the water friction gradient curves.

The close range covered by the predicted friction gradient curves for the Bingham, yield pseudoplastic and Newtonian curves (Figs. 9.44 & 9.45) makes immediate identification difficult. However, an investigation of the size distribution relative to the size analysis of the slurries tested in Chapter 7 should nevertheless allow the expected response to be assumed as Newtonian or non-Newtonian.

All the slurries tested in this chapter displayed settling characteristics. This result would then corroborate the assumption that stable flow only occurs when a minimum settling rate and/or minimum yield stress occurs⁽¹⁵⁾.

The concentration range of the slurries tested in this chapter are summarized in the following Table.

Table 9.56 Concentration range of medium phase slurries tested, the corresponding yield stress range measured and maximum particle size that can be transported as a stable slurry

Slurry type	C_w range (%)	C_v range (%)	Yield stress range (Pa)	Maximum particle size* for stable flow (μm)
Tails 14	47,3 - 66,0	22,9 - 39,1	,7 - 1,0	458 - 828
Tails 15	30 - 60,2	13,7 - 35,8	-	-
HMC	26 - 61,4	7,8 - 26,6	-	-
PFA	45 - 56	26,8 - 36,4	,52 - 1,7	588 - 2220
BBA	19 - 35	9,0 - 18,6	-	-
PFA/BBA	50 - 55	30,7 - 35,2	,79 - 1,7	926 - 2134
Tails 16	59 - 67,7	34,5 - 43,4	,3 - ,5	214 - 519
Tails 17				

* The calculation of the maximum particle size is based on equation 5.160.

It is clear from the above Table that the minimum yield stress requirement is not solely responsible for determining the stability of any slurry and would appear to be a function of the actual concentration, the maximum packing density, the quantity of fines, the interparticle contact and the forces which may exist between the particles and between the particles and the carrier.

As shown in the subsections in this chapter all the slurries exhibited a critical deposit velocity. The critical deposit velocity is clearly influenced by the particle size and specific gravity, the carrier medium concentration and rheological properties. This is clearly demonstrated in Section 9.6 where the BBA mixtures had a higher settling velocity than the PFA. The increasing ratio of PFA:BBA resulted in a reduction of the critical deposit

velocity. The result is dependent on the carrier concentration. The influence of the carrier rheology is illustrated in the 1:1 mixtures where the deposit velocity recorded for the $C_w = 40\%$ slurry is higher than the $C_w = 50\%$ slurry. The introduction of a fines carrier also has a beneficial effect on the friction gradient (Fig. 9.46).

The results indicated that in the medium phase region a number of characteristics are evident.

- 1) Slurry volume concentrations of the order of 8% - 43,4% for the particle size ranges tested are pumpable. The slurries tested represent the cross-section of materials conventionally transported as more dilute slurries.
- 2) The slurries all have critical deposit velocities. The transition from full flow characteristics to transportation with a deposited layer extends over a larger velocity range for the smaller particle slurries than the larger particle slurries.
- 3) The transport characteristics of a coarse material slurry is enhanced by the introduction of fine particles that mix with the carrying medium. The minimum transport velocity and pressure gradients are reduced with the introduction of the fine material.